



Uncollapsed LaFe_2As_2 phase: Compensated, highly doped, electron-phonon-coupled, iron-based superconductor


Ilaria Pallecchi ^{1,*}, Akira Iyo ², Hiraku Ogino,² Marco Affronte,³ and Marina Putti^{4,1}

¹CNR-SPIN, c/o Dipartimento di Fisica, via Dodecaneso 33, 16146 Genova, Italy

²National Institute of Advanced Industrial Science and Technology (AIST), 1-1-1 Umezono, Tsukuba, Ibaraki 305–8568, Japan

³Dipartimento di Scienze Fisiche, Informatiche e Matematiche, Università degli Studi di Modena e Reggio Emilia, and CNR-NANO, via G. Campi, 213/A, 41100 Modena, Italy

⁴Università di Genova, Dipartimento di Fisica, via Dodecaneso 33, 16146 Genova, Italy

 (Received 4 August 2020; revised 15 October 2020; accepted 9 November 2020; published 19 November 2020)

The recently discovered LaFe_2As_2 superconducting compound, member of the 122 family of iron pnictide superconductors, becomes superconducting below $T_c \approx 13$ K, yet its nominal doping apparently places it in the extreme overdoped limit, where superconductivity should be suppressed. In this work, we investigate the normal state of magneto- and thermoelectric transport and specific heat of this compound. The experimental data are consistent with the presence of highly compensated electron and hole bands, with ~ 0.42 electrons per unit cell just above T_c , and high effective masses $\sim 3m_0$. The temperature dependence of transport properties strongly resembles that of conventional superconductors, pointing to a key role of electron-phonon coupling. From this evidence, LaFe_2As_2 can be regarded as the connecting compound between unconventional and conventional superconductors.

DOI: [10.1103/PhysRevMaterials.4.114803](https://doi.org/10.1103/PhysRevMaterials.4.114803)

I. INTRODUCTION

Dome-shaped phase diagrams are a distinct hallmark of unconventional superconductivity. Iron-based superconductors are no exception to this rule. Specifically, in the so-called 122 family, with general composition $A\text{Fe}_2\text{As}_2$ (A = alkaline-earth metal), superconductivity occurs in a doping range below ~ 0.2 electrons/Fe [1]. This assumption was apparently challenged when the new stoichiometric compound LaFe_2As_2 was synthesized and found to be superconducting below ~ 12 K [2]. Indeed, this compound has a nominal doping of 0.5 electrons/Fe, which would place it in the dramatically overdoped regime, where superconductivity should be suppressed. Studying such odd one out may unveil the mysteries of unconventional superconductivity in iron pnictides.

Both LaFe_2As_2 and its isostructural CaFe_2As_2 derivative exist in two distinct crystallographic phases, namely the “collapsed” phase with shorter c axis and the “uncollapsed” phase with elongated c axis, and bulk superconductivity appears around ~ 12 K in just one of these two phases [2–4]. Indeed, the structural instability between collapsed and uncollapsed phases is typical of $A\text{Fe}_2\text{As}_2$ compounds (A = alkali or alkaline-earth metal), where the drastic changes in lattice parameters are accompanied by significant changes of the electronic properties, related to the underlying changes of the dimensionality of the electronic band structure and changes of the Fe magnetic moment [5,6]. In the case of LaFe_2As_2 , the as-synthesized collapsed compound is not superconducting, while the 500 °C annealed uncollapsed compound is, yet none

of the two phases exhibits long-range magnetic ordering [2]. The phase diagram of the uncollapsed system was explored in the chemically substituted $(\text{La}_{0.5-x}\text{Na}_{0.5+x})\text{Fe}_2\text{As}_2$ compound [7,8]. Here, the formal valence of FeAs layer is controlled linearly by the single parameter x from hole-doping ($x > 0$) to electron-doping ($x < 0$) region, with $x = 0$ corresponding to the Fe formal valence +2, typical of Fe-pnictides parent compounds. Indeed, stripe-type antiferromagnetic order below $T_N = 130$ K was found for $x = 0$, while superconductivity of multigap nature was found below $T_c \sim 9.4$ K and $T_c \sim 27$ K for $x = -0.5$ and $x = +0.3$, respectively. On the other hand, no intrinsic bulk superconductivity was detected in $\text{La}_{0.4}\text{Na}_{0.6}\text{Fe}_2\text{As}_2$ by either Co doping or application of pressure, even if in both cases suppression of the antiferromagnetic ordering was obtained [9].

To shed light on this system, structural, magnetic, and electronic properties of LaFe_2As_2 were calculated *ab initio* by Mazin *et al.* [10], indicating that the uncollapsed phase carries a strong short-range magnetism, which ultimately drives the superconducting transition. The puzzle related to the absence of any hole pockets near the zone center [2,7], which is virtually ubiquitous in superconducting iron pnictides, was solved by calculations that showed that the orbitals relevant for the low-energy physics are not the usual d_{xz} and d_{yz} , which are almost completely filled, but rather the d_{xy} and d_z ones [10]. Indeed, d_{xy} orbital forms a quasi-two-dimensional cylinder at the zone center, much resembling the hole pocket in other iron pnictides [10,11]. Experimental evidence of such hole pockets is argued [2,7], yet still lacking so far. As for the puzzle of dramatic overdoping, in the calculated band structure, the $5d_{xy}$ orbital is strongly hybridized with the As $4p$ orbital and has a huge dispersion [10] and both these factors cause an

*ilaria.pallecchi@spin.cnr.it

absorption of electrons by other bands well below the Fermi level, determining a reduced effective doping, as compared to the nominal 0.5 electrons/Fe. Even if the exact number of carrier could not be estimated precisely, due to strong hybridization, upper and lower limits of 0.47 and 0.22 electrons/Fe were given in Ref. [10], which certainly places the compound in the overdoped regime, but well below 0.5 electrons/Fe.

Further insight into the plausible pairing mechanisms of LaFe_2As_2 were given from *ab initio* calculations of Ref. [12], where the proximity of the narrow Fe d_{xy} band to the Fermi level was identified as a key feature for the appearance of superconductivity in the uncollapsed phase of LaFe_2As_2 , with respect to the collapsed phase. In this work [12], it was suggested that correlation and enhanced scattering in the d_{xy} band result in intense low-energy spin fluctuations, that provide glue for unconventional Cooper pair formation.

In this scenario, an experimental input is necessary to find a place for superconducting LaFe_2As_2 in a doping- T_c phase diagram and possibly reconcile its description with that of other iron pnictides.

In this work, we measure normal-state transport properties and specific heat in polycrystalline uncollapsed LaFe_2As_2 samples, and find evidence of electron and hole bands with high effective masses contributing to transport. We extract electronic parameters in a two-band framework and find that this compound is highly overdoped and highly compensated. While the compensated character makes LaFe_2As_2 akin to other iron-based superconductors, such as isovalent substituted chalcogenides [13,14], the highly overdoped character and the distinctive temperature dependence of resistivity and Seebeck coefficient typical of phonon-mediated superconductors make it the odd one out among iron-based superconductors.

II. MAGNETOELECTRIC AND THERMOELECTRIC TRANSPORT PROPERTIES

Uncollapsed LaFe_2As_2 samples were synthesized using a high-pressure and high-temperature synthesis method with subsequent annealing as described in Ref. [2]. Magnetotransport and Seebeck measurements were carried out in a Physical Property Measurement System (PPMS) by Quantum Design, in applied magnetic fields up to 9 T and at temperatures down to 5 K. Two samples were fully characterized. Since very similar behavior was observed in the two samples, in this paper we present data on one of them.

A. Resistivity

In Fig. 1, the metallic resistivity of LaFe_2As_2 is shown. The room-temperature resistivity is $80 \mu\Omega \text{ cm}$ and the residual resistivity is on the order $1 \mu\Omega \text{ cm}$, so that a residual resistivity ratio ~ 80 can be evaluated. Notably, the resistivity does not flatten in the temperature range just above T_c , indicating that scattering by phonons is the dominant mechanism, even at the lowest temperatures.

The onset of superconductivity is at $T_c = 13.1 \text{ K}$ and the transition width is $\sim 1 \text{ K}$. In the upper left inset, the resistive transition at different applied fields is shown. With applied

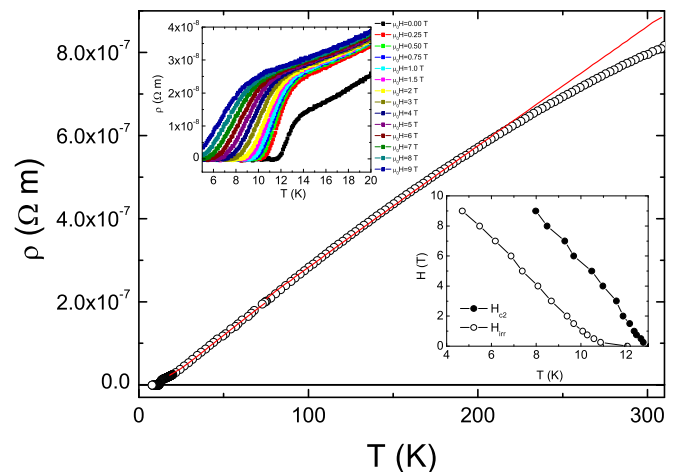


FIG. 1. Resistivity of LaFe_2As_2 . The continuous red line represents the fit with the generalized Bloch-Grüneisen law, Eq. (1). Upper left inset: resistivity curves in different magnetic fields up to 9 T. Lower right inset: H_{c2} and H_{irr} extracted from the resistive transitions with the criteria of 90 and 10% of the normal state resistivity, respectively.

field, the transition onset shifts monotonically to lower temperatures and the transition width increases monotonically, as it is visible in the plot of upper critical field H_{c2} and irreversibility field H_{irr} , in the lower right inset of Fig. 1. The H_{c2} and H_{irr} slopes are -1.82 and -1.38 T/K , in agreement with Ref. [2]. The upper inset in Fig. 1, presenting zero-field and in-field transitions, also shows a well-visible departure of normal state resistivity of the zero-field curve from those in field. On the other hand, for all the curves measured in fields equal to or larger than 0.25 T the resistivity changes very little with applied field. This behavior was observed in both our measured samples.

As shown in the main panel of Fig. 1, the resistivity curve in the normal state is described by a generalized Bloch-Grüneisen law, typical of metals [15,16]:

$$\begin{aligned} \rho(T) &= \rho_0 + \rho_{ph}(T) \quad \text{with} \\ \rho_{ph}(T) &= (m-1)\rho' \Theta_R \left(\frac{T}{\Theta_R} \right)^m \\ &\quad \times \int_0^{\Theta_R/T} \frac{z^m}{(1-e^{-z})(e^z-1)} dz. \end{aligned} \quad (1)$$

In the low-temperature range $T < 35 \text{ K}$, the experimental resistivity curve follows a power law $\rho(T) = \rho_0 + \text{const} \times T^m$ with $\rho_0 \sim 1 \mu\Omega$ and $m \sim 3$. A similar behavior has been observed in MgB_2 and it is typical of multiband systems [17]. By fixing $m = 3$, the temperature range up to $\sim 220 \text{ K}$ can be fitted with Eq. (1), while at higher temperatures, the experimental curve bends with respect to the Bloch-Grüneisen law. This tendency to saturation has been observed in A15 superconductors [18,19] and it is typical of metals with large electron-phonon coupling; indeed, when the resistivity rises steeply with increasing temperature, the mean-free path decreases and approaches the lattice spacing, which sets a limit for further increase of resistivity, according to the Ioffe-Regel criterion [20]. We estimate that the mean-free path at 300 K is $\sim 1 \text{ nm}$, comparable to the lattice parameters [2].

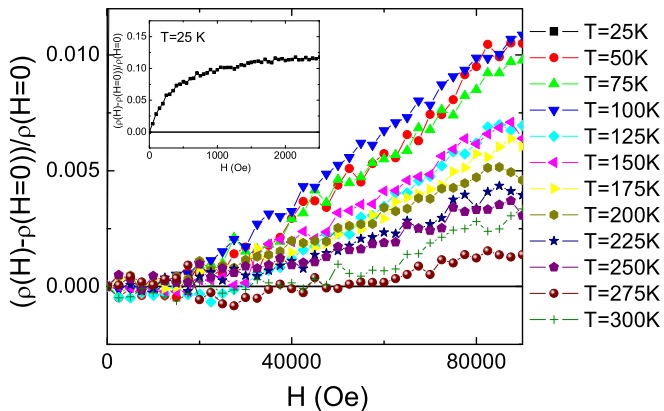


FIG. 2. Isothermal magnetoresistivity of LaFe₂As₂ at different temperatures. The curve at 25 K is shown in the inset magnifying the low-field regime.

B. Magnetoresistance and Hall effect

Figure 2 displays isothermal magnetoresistivity $[\Delta\rho(H) - \rho(H=0)]/\rho(H=0)$, measured at different temperatures from 25 to 300 K. At all the temperatures, magnetoresistivity is positive. For temperatures ≥ 50 K, $\Delta\rho$ decreases in magnitude with decreasing temperature, being around 1% at 9 T and 50 K and 0.25% at 9 T and room temperature. These curves can be described by the semiclassical model of magnetoresistivity proportional to the B^2 . The curve at 25 K, magnified in the low-field range in the inset of Fig. 2, exhibits a different behavior which cannot be described in the semiclassical cyclotron framework, and is rather reminiscent of a weak antilocalization mechanism, with a sharp dip at low field and saturation at higher fields. The magnitude of $\Delta\rho$ is larger than 10%, for fields above 0.25 T, which is reconciled with the behavior of resistive transitions presented above (see upper left inset of Fig. 1). This behavior disappears with increasing temperature, so that above 50 K only the cyclotronic mechanisms survives.

The Hall resistance curves measured at different temperatures are presented in Fig. 3. The slope is negative, indicating that the dominant charge carriers are electrons. However, the most noteworthy feature is the well-visible nonlinearity, at

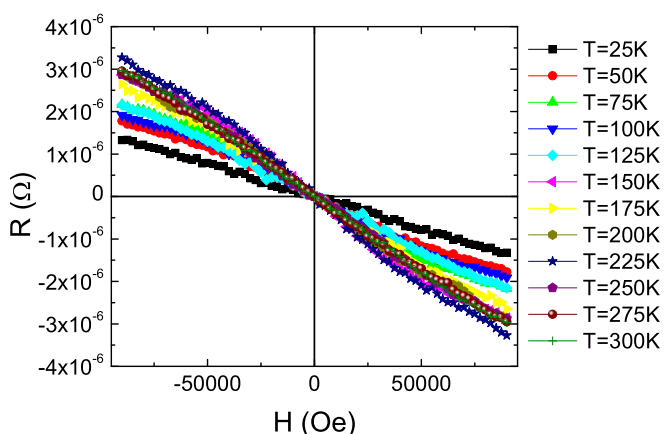


FIG. 3. Hall resistance of LaFe₂As₂ at different temperatures.

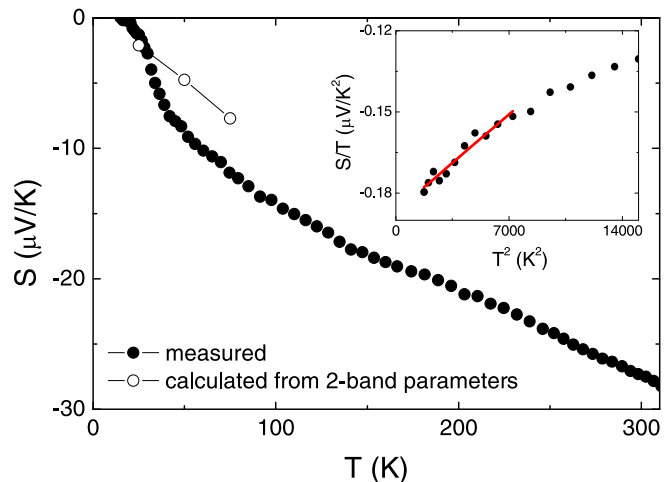


FIG. 4. Measured Seebeck coefficient of LaFe₂As₂ (filled symbols). The diffusive Seebeck coefficient calculated from the two-band parameters is also shown in the main panel (open symbols). Inset: S/T vs T^2 plot, with a linear regime identified in correspondence of the temperature range 40–85 K, as described by Eq. (2), with fitting parameters $A \approx -0.186 \mu\text{V}/\text{K}^2$ and $B \approx 5.13 \times 10^{-6} \mu\text{V}/\text{K}^4$.

all the temperatures except for 25 K. Such nonlinearity is an unambiguous evidence of the presence of a hole band at the Fermi level, which participates in transport, as it is the case of most of the other 122 superconducting compounds.

C. Seebeck Effect

In Fig. 4, the temperature dependence of the Seebeck coefficient S of LaFe₂As₂ is presented. The negative sign of S is consistent with the negative sign of the Hall effect. The monotonic temperature dependence of S and its small value $\sim 27.5 \mu\text{V}/\text{K}$ at 300 K are consistent with the metallic character of this compound. More specifically, as for most clean metals, S is composed of a linear diffusive contribution plus a broad bump at low temperatures, centered around 50–60 K in Fig. 4, which can be ascribed to a phonon drag contribution. For temperatures much smaller than the Debye temperature Θ_D the phonon drag Seebeck coefficient is expected to be proportional to the phonon contribution to the specific heat [21], thus behaving as $\sim T^3$. We then assume that the experimental S is a sum of the diffusive Seebeck $\propto T$ plus the phonon drag Seebeck $\propto T^3$, as previously done for the conventional superconductor MgB₂ [15]:

$$S = AT + BT^3. \quad (2)$$

Plotting S/T vs T^2 , as in the inset of Fig. 4, we can identify a linear regime in the 40–85 K temperature range and extract the diffusive and phonon drag coefficients A and B , as the intercept and the slope, respectively. The obtained values are $A \approx -0.186 \mu\text{V}/\text{K}^2$ and $B \approx -5.13 \times 10^{-6} \text{mV}/\text{K}^4$. Considering now the B coefficient which represents the amplitude of the phonon drag term, we note that the ratio $B/A \approx 3 \times 10^{-5} \text{K}^{-2}$ is of the same order as the corresponding ratio in MgB₂ ($B/A \approx 7 \times 10^{-5} \text{K}^{-2}$) [15]. This observation of a Seebeck term proportional to T^3 with a reliable order of magnitude is

clear evidence that phonon drag contributes significantly to Seebeck effect; this generally occurs in pure metals with strong electron-phonon coupling, where phonon scattering is the dominant interaction of electrons, as for the case of MgB₂.

III. SPECIFIC-HEAT MEASUREMENTS

Heat-capacity measurements were performed with a PPMS system of the Quantum Design on a polycrystalline sample of mass 71.8 mg by the relaxation method with typical temperature pulse of $\Delta T \approx 1\%$ with respect to the bath temperature.

In Fig. 5, the temperature dependence of the specific heat c is presented. The lower right inset shows that the c value, normalized to the universal gas constant R , tends to saturate at high temperature at a value slightly larger than $15R$, as expected from the Dulong-Petit law for the lattice contribution $3xN_{\text{at}}xR$ where $N_{\text{at}} = 5$ is the number of atoms per unit cell. The excess to this value obviously comes from the electronic and magnetic contributions.

The molar specific heat c measured in zero field and in a 7-T field below 20 K, is plotted as c/T vs the squared temperature T^2 in the main panel of Fig. 5. Below T_c , the zero-field data exhibit an onset of a broad bump, related to the superconducting transition. For the 7-T data, the transition is broadened and is shifted to lower temperatures. These zero-field and in-field superconducting transitions are better evidenced in the plot of the electronic superconducting contribution to the specific heat $c_{\text{es}}/T = c/T - (\gamma + \beta T^2)$ vs T , shown in the upper left inset of Fig. 5. It is seen that the onsets of the transitions are consistent with the H_{c2} data extracted from the superconducting onsets of the resistivity curves (lower right

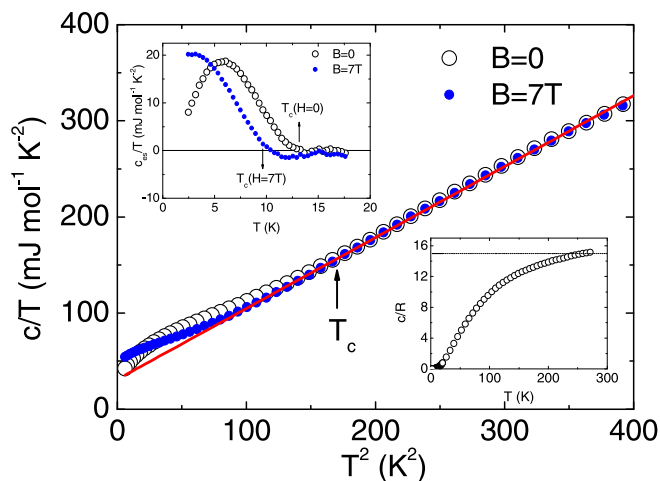


FIG. 5. Specific heat c of LaFe₂As₂ in zero field and in a 7-T field, plotted as c/T vs T^2 . The continuous red line represents a linear fit to the 7-T data in the temperature range between T_c and 20 K, with best-fit coefficients $c/T[\text{mJ mol}^{-1} \text{K}^{-2}] = (35 + 0.73T^2)[\text{mJ mol}^{-1} \text{K}^{-2}]$. In the upper left inset, the electronic superconducting contribution to the specific heat $c_{\text{es}}/T = c/T - (\gamma + \beta T^2)$, which better evidences the superconducting transition, is plotted vs T . In the lower right inset, c in units of R is plotted vs T and the horizontal dashed line represents the value $3 \times N_{\text{at}} \times R = 15R$, expected from the Dulong-Petit law for the lattice contribution.

inset of Fig. 1), indicated by arrows at $T_c \approx 13$ K in zero field and at $T_c \approx 9.5$ K in 7-T field.

Between 10 and 20 K, the in-field $c(7\text{-T})$ data in the normal state fits well the law:

$$c(T) = \gamma T + \beta T^3, \quad (3)$$

where γ is the electronic specific heat, also known as Sommerfeld coefficient, and the $c/T \propto T^2$ term is the Debye contribution of acoustic phonons. The best fit of 7-T data between 10 and 20 K gives $\gamma \approx 35 \text{ mJ mol}^{-1} \text{K}^{-2}$ and $\beta \approx 0.73 \text{ mJ mol}^{-1} \text{K}^{-4}$, with a 5% uncertainty on both coefficients γ and β related to slight variations of the fitting range. The molar electronic specific heat $\gamma \approx 35 \text{ mJ mol}^{-1} \text{K}^{-2}$ is quite large a value for a good metal, indicative of a high effective mass. The slope $\beta = 0.73 \text{ mJ mol}^{-1} \text{K}^{-4}$ is related to the phonon spectrum and, in the low-temperature limit where only acoustic phonons contribute to the specific heat, it is related to the Debye temperature Θ_D by the relation

$$\Theta_D = \sqrt[3]{\left(\frac{12}{5}\pi^4 R\right)/\beta}. \quad (4)$$

From Eq. (4), we obtain for the Debye temperature $\Theta_D \approx 140$ K.

We finally note that in the upper left inset of Fig. 5 the magnitude of c_{es}/T maximum is around $20 \text{ mJ mol}^{-1} \text{K}^{-2}$. Considering that for a homogeneous BCS superconductor, the difference between superconducting and normal electron contributions to specific heat at T_c normalized to γT_c is expected to be $\frac{c_{\text{es}}(T_c)}{\gamma T_c} \approx 1.43$, our values point to a bulk superconductor, although not fully homogeneous.

IV. DATA ANALYSIS AND DISCUSSION

A. Carrier densities and mobilities

Normal state magnetotransport is revealing of band parameters if analyzed in the proper framework, thus offering the opportunity of clarifying the real nature of this apparently peculiar member of the 122 iron-based superconductors. We first analyze data in a simple single-band framework. In the upper panel of Fig. 6, carrier density and mobility are extracted, respectively, from the linear fit of Hall resistance curves and from the inverse product of carrier density and resistivity. The carrier density varies from $2 \times 10^{22} \text{ cm}^{-3}$ at 25 K to $9 \times 10^{21} \text{ cm}^{-3}$ at 300 K. Temperature dependence of carrier density is not expected in a single-band framework. In addition, the absolute values are unrealistically large, the 25 K values pointing to 3.5 electrons per unit cell. These two observations, together with the nonlinearity Hall resistance curves (see Fig. 3), indicate that the single-band description is inadequate; thereby a two-band analysis, with one electron band and one hole band, must be carried out, instead. In order to determine carrier densities and mobilities of the two bands, n_e , n_h , μ_e , and μ_h at each fixed temperature, we need four equations. The expression of the nonlinear Hall resistance is written as

$$R_{xy} = \frac{\text{Vol} (-\mu_e^2 n_e + \mu_h^2 n_h) + (-n_e + n_h)(\mu_e \mu_h B)^2}{q (\mu_e n_e + \mu_h n_h)^2 + (-n_e + n_h)^2 (\mu_e \mu_h B)^2} B, \quad (5)$$

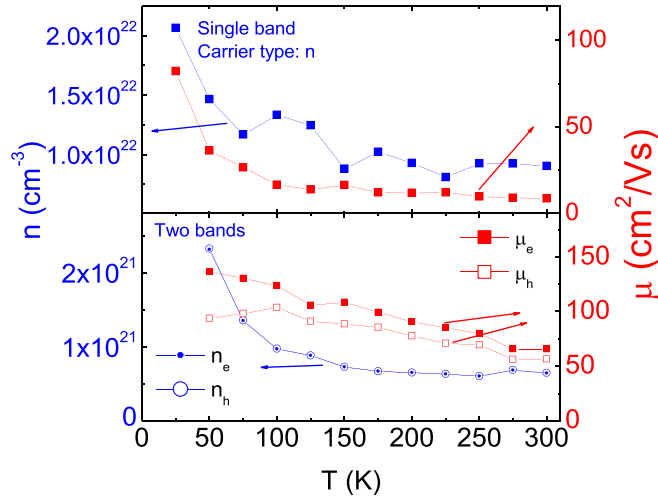


FIG. 6. Carrier concentrations and mobilities extracted from data analysis in a single-band framework (upper panel) and in a two-band framework (lower panel).

where the sign of the charge carriers is already made explicit, so that the parameters n_e , n_h , μ_e and μ_h are all positive. In Eq. (5), Vol is the unit-cell volume, q is the positive electronic charge, and B is the applied field in tesla. Despite fitting the experimental curves of Fig. 3 with Eq. (5) could in principle provide three coefficients and thus three equations, our experimental curves can be well fitted by just two parameters:

$$R_{fit} = \frac{\alpha B + \xi B^3}{1 + \delta B^2} \approx \alpha \mu_0 B + (\xi - \alpha \delta) B^3, \quad (6)$$

where the tentative assumption $\delta B^2 \ll 1$ is done. We obtain the other two equations from the values of resistivity and of cyclotron magnetoresistivity at 9 T, expressed, respectively, as

$$\rho = \frac{Vol}{q} \frac{1}{\mu_e n_e + \mu_h n_h}, \quad (7)$$

$$\frac{\rho(B) - \rho(0)}{\rho(0)} \approx \frac{n_e n_h \mu_e \mu_h (\mu_e + \mu_h)^2}{(\mu_e n_e + \mu_h n_h)^2} B^2. \quad (8)$$

Note that Eq. (8) is truncated at the leading order in B^2 , as applicable to the low magnetoresistivities in Fig. 2. Note also that in Eq. (8) contribution of bands of different signs (holes and electrons) are additive, while contributions of bands of the same sign would subtract as $\propto (\mu_1 - \mu_2)^2$.

Hence, by combining the equations for the linear and cubic fitting coefficients of R_{xy} given by Eqs. (5) and (6), for ρ given by Eq. (7) and for $\frac{\rho(B=9T) - \rho(0)}{\rho(0)}$ given by Eq. (8), we obtain n_e , n_h , μ_e , and μ_h at each temperature, as displayed in the bottom panel of Fig. 6. The datum at 25 K is missing because we have neither the cyclotron magnetoresistance (see inset of Fig. 2) nor the nonlinear Hall resistance coefficient $(\xi - \alpha \delta)$ in Eq. (6), as the Hall resistance at 25 K is linear in the field (see Fig. 3). Note that the solution is not univocal in principle, because the experimental curvature of the flex point in the R_{xy} curve can be reproduced with infinite choices of the parameters ξ and δ ; however, solutions are only found for $\delta \ll \xi/\alpha$ (and $\delta B^2 \ll 1$, as assumed *a priori*), that is for

$R_{fit} \approx \alpha \mu_0 B + \xi B^3$ in Eq. (6). Note also that by dropping the assumption $\delta B^2 \ll 1$, and assuming instead $\xi \ll \alpha/B^2$, that is using the fitting equation $R_{fit} = \frac{\alpha B + \xi B^3}{1 + \delta B^2} \approx \frac{\alpha B}{1 + \delta B^2}$, no solution is found for n_e , n_h , μ_e , and μ_h . We also tried to analyze data by assuming two electron bands, but no solution was found in this case either, thus confirming the existence of a hole-band contribution to transport.

From these results we conclude that: (i) LaFe₂As₂ is a highly compensated compound, with carrier densities of the hole- and electron bands that differ by around 1%; (ii) the carrier densities of the hole- and electron bands are ~ 0.42 electrons per unit cell at 50 K and ~ 0.12 electrons per unit cell at room temperature; hence, in the highly overdoped regime at low temperature $T = 50$ K; (iii) electron mobility is larger than hole one by a factor of 1.5 at low temperature and 1.2 at room temperature, with both μ_e and μ_h decreasing by a factor of ~ 2 in this temperature range. The compensation up to $\sim 99\%$ of hole- and electron bands needs to be further discussed. Although charge compensation is not unusual in iron-based superconductors [13,14], compensation up to $\sim 99\%$ is quite remarkable. On the other hand, the extremely low experimental values of the Hall effect, measured in both our samples, can be explained only by either unrealistically large carrier densities, as in the single-band analysis, or by very high carrier compensation of bands of different signs. The latter seems to be the case, as indicated by our analysis with no free parameters. Such high degree of compensation should yield nonsaturating quadratic magnetoresistance up to very high fields ≥ 35 T, which should be checked in future experiments.

B. Effective masses

The effective mass can be extracted from the Sommerfeld coefficient γ , which can be expressed as the sum of electron and hole contributions γ_e and γ_h as

$$\gamma = \gamma_e + \gamma_h = \frac{\pi^2 K_B^2 N_{av}}{2} \left(\frac{1}{E_{F(e)}} + \frac{1}{E_{F(h)}} \right), \quad (9)$$

where N_{av} is the Avogadro number and E_F the Fermi energy, which for three-dimensional parabolic bands can be expressed as $E_F = \frac{\hbar^2}{2m_{eff}} (3\pi^2 n)^{2/3}$. From the two-band analysis it turns out that electron and hole mobilities are nearly equal; therefore, it is reasonable to assume nearly equal effective masses $m_{eff(e)} \approx m_{eff(h)}$, which implies nearly equal Fermi energies, given that $n_e \approx n_h$. Hence the value $\gamma = (35 \pm 2) \text{ mJ mol}^{-1} \text{ K}^{-2}$ found from specific heat is reproduced by assuming effective masses $m_{eff(e)} \approx m_{eff(h)} \approx 3m_0$. This m_{eff} value is similar to what is on average obtained from de Haas–van Alphen [22] and angle resolved photoemission spectroscopy [23] measurements on 122 superconductors.

The analysis of the Seebeck effect provides additional information. The diffusive contribution to the Seebeck coefficient can be calculated in the two-band framework. The conductivities σ_e and σ_h weigh the sum of band contributions S_e and S_h to the Seebeck coefficient, according to the expression

$$S = \frac{\sigma_e S_e + \sigma_h S_h}{\sigma_e + \sigma_h}. \quad (10)$$

In Eq. (10), the diffusive contributions of electron and hole bands to the Seebeck coefficient can be expressed by the Mott formula for metals, predicting a linear temperature dependence:

$$S_d = \pm \frac{\pi^2 K_B^2 T}{3q} \frac{\sigma'}{\sigma}, \quad (11)$$

where K_B is the Boltzmann constant, the sign $+/-$ applies to holes/electrons, and σ and σ' are the conductivity and its energy derivative calculated at the Fermi level E_F . By expressing σ and σ' with the Drude formula, the ratio σ'/σ results in the sum of logarithmic derivatives of carrier density $\partial \ln(n)/\partial E$ and of scattering time $\partial \ln(\tau)/\partial E$. Given the energy dependence of the density of states $N(E) \propto E^{1/2}$, we get $\partial \ln(n)/\partial E = 3/2$. The energy dependence of τ can be modeled by a power law τ^η , where the exponent η depends on the scattering mechanism and it is $\eta = -1/2$ for scattering by acoustic phonons [$\partial \ln(\tau)/\partial E = -1/2$] and $\eta = 0$ for scattering by impurities. With these assumptions, Eq. (11) is written as

$$S_d = \pm \left(\frac{3}{2} + \eta \right) \frac{\pi^2 K_B^2}{3q} T \frac{1}{E_F}. \quad (12)$$

Finally introducing the Fermi energy expression, the two-band diffusive Seebeck coefficient in Eq. (10) can be written in terms of the band parameters n_e , n_h , μ_e , μ_h and $m_{\text{eff}(e)} \approx m_{\text{eff}(h)}$ as

$$S_d = C \times T \times \frac{(n_e^{1/3} \mu_e \frac{m_{\text{eff}(e)}}{m_0}) - (n_h^{1/3} \mu_h \frac{m_{\text{eff}(h)}}{m_0})}{n_e \mu_e + n_h \mu_h}, \quad (13)$$

where $C = \left(\frac{3}{2} + \eta \right) \frac{\pi^2 K_B^2}{3q} \frac{2m_0}{\hbar^2 (3\pi^2)^{2/3}}$ is a dimensional constant and m_0 is the bare electron mass.

Using the two-band parameters extracted from the fit of specific heat and magnetotransport data, the diffusive Seebeck coefficient S_d can be calculated by Eq. (13). This calculated S_d is plotted as open symbols in Fig. 4, assuming $\eta = 0$ in the low-temperature limit of scattering by impurities. Notably, given the strong compensation between the electron and hole contribution which suppresses S_d , the consistency between the measured S and S_d , can be obtained only with large effective masses, at least $\sim 3m_0$; hence, the analysis of the Seebeck curve is an independent and consistent evaluation of m_{eff} .

We can now compare the slope of the linear fit $dS_d/dT \approx -0.11 \mu\text{V}/\text{K}^2$ of diffusive Seebeck calculated by Eq. (13) with the intercept $A \approx -0.19 \mu\text{V}/\text{K}^2$ evaluated by Eq. (2) from the temperature dependence of the Seebeck effect. The magnitude of A is larger than dS_d/dT ; however this is pretty plausible, considering that the linear temperature dependence predicted by the Mott law is itself an oversimplification, which does not describe experimental data when different scattering mechanisms come into play across the temperature range [24] and possible renormalization effects [15,25].

C. Electron-phonon coupling constant

So far, we collected several pieces of evidence of the prominent role of electron-phonon coupling in this LaFe_2As_2 making it mandatory to give an estimation of the electron-phonon coupling from transport properties. An approximate

evaluation of the transport electron-phonon coupling λ_{tr} can be obtained by the resistivity coefficient ρ' in Eq. (1), which can be expressed as [15]

$$\rho' = \frac{m_{\text{eff}}}{nq^2} \frac{2\pi K_B}{\hbar} \lambda_{\text{tr}}. \quad (14)$$

Therefore λ_{tr} can be evaluated using the values of carrier density and effective mass as in the above analysis and the coefficient ρ' extracted by the Bloch-Grüneisen fit. Although the Bloch-Grüneisen law apparently fits resistivity data up to ~ 220 K, it describes the coupling of charge carriers with the acoustic phonons only. Thus, for consistency, we limit the fitting of resistivity by Eq. (1) to the low-temperature T^3 range, characteristic of coupling of charge carriers with acoustic phonons, also seen in specific-heat data. The best-fit parameters are Debye temperature $\Theta_D \approx 200$ K and $\rho' \approx 1 \mu\Omega\text{cm}$. The Debye temperatures $\Theta_D \approx 140$ K and $\Theta_R \approx 200$ K extracted from specific heat and resistivity, respectively, are in substantial agreement. With this ρ' value, from Eq. (14) we find $\lambda_{\text{tr}} \approx 0.11$. This value is close to the electron-phonon coupling constant ~ 0.21 calculated for 1111 iron-pnictide compounds [26] and ~ 0.18 calculated for 122 compounds [27]. We point out that our experimental estimate refers to the coupling with acoustic phonons only, neglecting the contribution of optical phonons. From this λ_{tr} value, the BCS evaluation of the critical temperature turns out negligible, suggesting that phonon coupling cannot be the main pairing mechanism in play. However, the relevance of the interaction with the phonons, emphasized by low impurity scattering, appears clearly from the analysis of the temperature dependence of normal state resistivity and Seebeck coefficient, placing this compound somewhat midway between conventional superconductors, such as A15 and MgB_2 , and its peers, iron-based unconventional superconductors. Indeed, even if it seems that in LaFe_2As_2 superconductivity is likely unconventional in nature, coupling with phonons could play a role, not only in the normal state, but also in the superconducting mechanisms, possibly accounting for the peculiar behavior of being superconducting far beyond the highly overdoped regime.

V. CONCLUSIONS

In this work, we present characterization of normal state transport and thermal properties of the LaFe_2As_2 superconducting compound, a highly metallic member of the 122 family of iron-based compounds. We combine specific heat, resistivity, magnetoresistivity, Hall effect, and Seebeck effect data to carry out a self-consistent data analysis in a two-band framework. We find evidence that although transport is dominated by an electron band, a hole band at the Fermi level does make a significant contribution to transport. Indeed, this compound is highly compensated, with electron and hole bands having equal carrier densities within $\sim 1\%$ and high effective masses $\sim 3m_0$. Most remarkably, this compound is highly overdoped, with ~ 0.42 electrons per unit cell at 50 K. This finding challenges the usual belief that the superconducting dome in the phase diagram of 122 iron-based superconductors typically ends in correspondence at 0.2 electrons per unit cell. As much remarkable, opposite to the behavior of its unconventional superconducting pnictide peers, normal state

transport in this compound exhibits some distinctive features of the phonon-coupled traditional superconductors, namely a Bloch-Grüneisen-type resistivity, an Ioffe-Regel saturation of resistivity at high temperatures, and a phonon drag contribution to the Seebeck effect. We estimate an electron-phonon coupling $\lambda_{\text{tr}} \approx 0.11$, too small to account for any role of phonons in the pairing mechanism. *Ab initio* calculations of the electronic structure in literature [10,12] indicate that this compound is similar to other 122 superconducting pnictides.

From these seemingly contrasting premises, the superconducting mechanisms in LaFe_2As_2 appear to be a puzzle and should be further investigated by theoretical and experimental approaches.

ACKNOWLEDGMENT

This work was supported by JSPS KAKENHI Grant No. JP16H6439.

- [1] F. Rullier-Albenque, Influence of the electronic structure on the transport properties of some iron pnictides, *C. R. Phys.* **17**, 164 (2016).
- [2] A. Iyo, S. Ishida, H. Fujihisa, Y. Gotoh, I. Hase, Y. Yoshida, H. Eisaki, and K. Kawashima, Superconductivity in uncollapsed tetragonal LaFe_2As_2 , *J. Phys. Chem. Lett.* **10**, 1018 (2019).
- [3] K. Prokeš, A. Kreyssig, B. Ouladdiaf, D. K. Pratt, N. Ni, S. L. Bud'ko, P. C. Canfield, R. J. McQueeney, D. N. Argyriou, and A. I. Goldman, Evidence from neutron diffraction for superconductivity in the stabilized tetragonal phase of CaFe_2As_2 under uniaxial pressure, *Phys. Rev. B* **81**, 180506(R) (2010).
- [4] M. S. Torikachvili, S. L. Bud'ko, N. Ni, and P. C. Canfield, Pressure Induced Superconductivity in CaFe_2As_2 , *Phys. Rev. Lett.* **101**, 057006 (2008).
- [5] E. Gati, L. Xiang, S. L. Bud'ko, and P. C. Canfield, Hydrostatic and uniaxial pressure tuning of iron-based superconductors: Insights into superconductivity, magnetism, nematicity and collapsed tetragonal transitions, *Ann. Phys.* **532**, 2000248 (2020).
- [6] A. Kreyssig, M. A. Green, Y. Lee, G. D. Samolyuk, P. Zajdel, J. W. Lynn, S. L. Bud'ko, M. S. Torikachvili, N. Ni, S. Nandi, J. B. Leão, S. J. Poulton, D. N. Argyriou, B. N. Harmon, R. J. McQueeney, P. C. Canfield, and A. I. Goldman, Pressure-induced volume-collapsed tetragonal phase of CaFe_2As_2 as seen via neutron scattering, *Phys. Rev. B* **78**, 184517 (2008).
- [7] T. Kouchi, M. Yashima, H. Mukuda, S. Ishida, H. Eisaki, Y. Yoshida, K. Kawashima, and A. Iyo, Unconventional multi-gap superconductivity and antiferromagnetic spin fluctuations in new Iron-arsenide LaFe_2As_2 in heavily electron-doped regime, *J. Phys. Soc. Jpn.* **88**, 113702 (2019).
- [8] A. Iyo, K. Kawashima, S. Ishida, H. Fujihisa, Y. Gotoh, H. Eisaki, and Y. Yoshida, Superconductivity on hole-doping side of $(\text{La}_{0.5-x}\text{Na}_{0.5+x})\text{Fe}_2\text{As}_2$, *J. Am. Chem. Soc.* **140**, 369 (2018).
- [9] X. Xing, M. Li, J. Feng, X. Yi, Y. Meng, B. Shen, and Z. Shi, Co doping and high pressure studies of the iron arsenide $\text{La}_{0.4}\text{Na}_{0.6}\text{Fe}_2\text{As}_2$, *J. Phys. Soc. Jpn.* **89**, 055001 (2020).
- [10] I. I. Mazin, M. Shimizu, N. Takemori, and H. O. Jeschke, Novel Fe-Based Superconductor LaFe_2As_2 in Comparison with Traditional Pnictides, *Phys. Rev. Lett.* **123**, 267001 (2019).
- [11] H. Usui and K. Kuroki, Hidden robust presence of a hole Fermi surface in a heavily electron-doped iron-based superconductor LaFe_2As_2 , *Phys. Rev. Res.* **1**, 033025 (2019).
- [12] S. Acharya, D. Pashov, F. Jamet, and M. van Schilfgaarde, Controlling T_c through Band Structure and Correlation Engineering in Collapsed and Uncollapsed Phases of Iron Arsenides, *Phys. Rev. Lett.* **124**, 237001 (2020).
- [13] I. Pallecchi, G. Lamura, M. Tropeano, M. Putti, R. Viennois, E. Giannini, and D. Van der Marel, Seebeck effect in $\text{Fe}_{1+x}\text{Te}_{1-y}\text{Se}_y$ single crystals, *Phys. Rev. B* **80**, 214511 (2009).
- [14] F. Caglieris, F. Ricci, G. Lamura, A. Martinelli, A. Palenzona, I. Pallecchi, A. Sala, G. Profeta, and M. Putti, Theoretical and experimental investigation of magnetotransport in iron chalcogenides, *Sci. Technol. Adv. Mater.* **13**, 054402 (2012).
- [15] M. Putti, E. Galleani d'Agliano, D. Marré, F. Napoli, M. Tassisto, P. Manfrinetti, A. Palenzona, C. Rizzuto, and S. Massidda, Electron transport properties of MgB_2 in the normal state, *Eur. Phys. J. B* **25**, 439 (2002).
- [16] I. Pallecchi, C. Belfortini, F. Canepa, C. Ferdeghini, P. Manfrinetti, A. Palenzona, R. Vaglio, and M. Putti, Nonsaturating linear resistivity up to 900 K in MgB_2 , *Phys. Rev. B* **79**, 134508 (2009).
- [17] G. T. Meaden, *Electrical Resistance of Metals* (Heywood Books, London, 1966), p. 89.
- [18] F. Nava, O. Bisi, and K. N. Tu, Electrical transport properties of V_3Si , V_5Si_3 , and VSi_2 thin films, *Phys. Rev. B* **34**, 6143 (1986).
- [19] M. Putti, R. Vaglio, and J. M. Rowell, Radiation effects on MgB_2 : A review and a comparison with A15 superconductors, *Supercond. Sci. Technol.* **21**, 043001 (2008).
- [20] A. F. Ioffe and A. R. Regel, Non-crystalline, amorphous and liquid electronic semiconductors, *Prog. Semicond.* **4**, 237 (1960).
- [21] J. M. Ziman, *Electrons and Phonons* (Clarendon Press, Oxford, 1960); R. D. Barnard, *Thermoelectricity in Metals and Alloys* (Taylor & Francis Ltd., London, 1972), p. 136.
- [22] J. G. Analytis, J.-H. Chu, R. D. McDonald, S. C. Riggs, and I. R. Fisher, Enhanced Fermi Surface Nesting in Superconducting $\text{BaFe}_2(\text{As}_{1-x}\text{P}_x)_2$ revealed by the de Haas-van Alphen Effect, *Phys. Rev. Lett.* **105**, 207004 (2010).
- [23] J. Li, Y.-F. Guo, Z.-R. Yang, K. Yamaura, E. Takayama-Muromachi, H.-B. Wang, and P.-H. Wu, Progress in nonmagnetic impurity doping studies on Fe-based superconductors, *Supercond. Sci. Technol.* **29**, 053001 (2016).
- [24] I. Pallecchi, M. Monni, P. Manfrinetti, and M. Putti, Band filling and disorder effects on the normal state thermoelectric behavior in MgB_2 , *J. Phys.: Condens. Matter* **31**, 164001 (2019).
- [25] G. Grimvall, The Electron-Phonon Interaction in Metals, edited by E. P. Wohlfarth, in *Selected Topics in Solid State Physics*, Vol. XVI (Elsevier, North-Holland, Amsterdam, The Netherlands, 1981); A. B. Kaiser, *Phys. Rev. B* **35**, 4677 (1987), and references therein.
- [26] L. Boeri, O. V. Dolgov, and A. A. Golubov, Is $\text{LaFeAsO}_{1-x}\text{F}_x$ an Electron-Phonon Superconductor? *Phys. Rev. Lett.* **101**, 026403 (2008).
- [27] L. Boeri, M. Calandra, I. I. Mazin, O. V. Dolgov, and F. Mauri, Effects of magnetism and doping on the electron-phonon coupling in BaFe_2As_2 , *Phys. Rev. B* **82**, 020506(R) (2010).